DEU FMD 28(83) (2026) 268-275

Dokuz Eylül Üniversitesi Mühendislik Fakültesi Fen ve Mühendislik Dergisi
Dokuz Eylul University Faculty of Engineering Journal of Science and Engineering
Elektronik/Online ISSN: 2547-958X

RESEARCH ARTICLE / ARAŞTIRMA MAKALESI

Petrographic and SEM-EDS Analyses of CAI Structures in Vigarano Type Carbonaceous Chondritic Meteorite NWA 5508

Vigarano Türü Karbonlu Kondritik Meteorit NWA 5508'deki CAI Yapılarının Petrografik ve SEM-EDS Analizleri

Ceren Kamil [1], Ozan Unsalan [2*], Osman Candan [3]

[1] Ege Üniversitesi Fen Bilimleri Enstitüsü, Malzeme Bilimi ve Mühendisliği Bölümü, İzmir, TÜRKİYE
[2] Ege Üniversitesi Fen Fakültesi, Fizik Bölümü, İzmir, TÜRKİYE
[3] Dokuz Eylül Üniversitesi, Mühendislik Fakültesi, Jeoloji Mühendisliği Bölümü, İzmir, TÜRKİYE

Corresponding Author / Sorumlu Yazar *: ozan.unsalan@ege.edu.tr

Abstract

Carbonaceous chondrites are the most primitive remnants of the early solar system, providing valuable information about the formation and evolution of the solar system. These extraterrestrial materials are rare and critical for understanding the conditions and processes that shaped the solar nebula. Vigarano-type carbonaceous meteorites are of particular importance since they contain unique Calcium-Aluminum-rich inclusions (CAIs), which are the earliest solids formed in the solar system and date back to 4.5 Ga. These inclusions provide fundamental clues about the environment of their origin. In addition, studying the mineralogical and chemical composition of carbonaceous chondrites and their potential source bodies is crucial, especially for the advancement of asteroid mining research. This study focuses on petrographic and scanning electron microscopy (SEM)-energy dispersive X-ray spectroscopy (EDS) analysis of the Vigarano-type NWA 5508 carbonaceous chondrite, known for its CAI-rich lithology.

Keywords: *Carbonaceous Chondrites, CAI, Petrography, Optical Microscopy, Scanning Electron Microscopy, Mineralogy*

Öz

Karbonlu kondritler, erken güneş sisteminin en ilkel kalıntılarıdır ve güneş sisteminin oluşumu ve evrimi hakkında değerli bilgiler sağlar. Nadir olarak bulunan bu dünya dışı malzemeler, güneş bulutsusunu şekillendiren koşulları ve süreçleri anlamak için kritik öneme sahiptir. Vigarano türü karbonlu meteoritler, güneş sisteminde oluşan en ilkel katılar olan ve 4,5 Ga'ya kadar uzanan benzersiz Kalsiyum-Alüminyum açısından zengin kapanımlar (CAI) içerdiklerinden özellikle önemlidir. Bu kapanımlar, kökenlerinin ortamı hakkında temel ipuçları sağlar. Ayrıca, karbonlu kondritlerin mineralojik ve kimyasal bileşimini ve potansiyel kaynak gövdelerini incelemek, özellikle asteroit madenciliği araştırmalarının ilerlemesi için çok önemlidir. Bu çalışma, CAI açısından zengin litolojisiyle bilinen Vigarano türü NWA 5508 karbonlu kondritinin petrografik ve taramalı elektron mikroskopisi (SEM)-enerji dağılımlı X-ışını spektroskopisi (EDS) analizine odaklanmaktadır.

Anahtar Kelimeler: *Karbonlu Kondritler, CAI, Petrografi, Optik Mikroskopi, Taramalı Elektron Mikroskopi, Mineraloji*

1. Introduction

Studies on meteorites offer profound insights into stellar evolution, the history of the solar nebula, Earth's geological past, the Moon's evolution, and the origins of life. Stony meteorites are the most common type of meteorite, accounting for 94% of observed meteorite falls and 86% of all meteorites found on Earth. Stony meteorites are divided into two distinct categories: chondrites, which contain rounded structures called chondrules, ranging in size from μm to cm, and achondrites, which do not. Carbonaceous chondrites, which are stony meteorites, are one of the most abundant extraterrestrial materials with primitive chemistry in the Solar System [1, 2]. Among meteorites, carbonaceous chondrites stand out as the most unaltered remnants of the early solar system, making their study critical for understanding both Earth's history and solar system formation and evolution. For instance, the age determination of stony meteorites from Antarctic ice has revealed the history of their origin back to 4.54 Ga, providing a precise estimate of the solar system's age [3]. In other work, the Murchison meteorite, a well-known carbonaceous chondrite, has yielded 96 amino acids, highlighting its significance in the study of prebiotic chemistry [4]. Similarly, research on organic compounds in carbonaceous chondrites and interplanetary dust particles has detailed the extraterrestrial formation mechanisms of these amino acids [5].

Carbonaceous asteroids, which are the parent bodies of carbonaceous chondrites, are important sources of the raw material that formed the approximately 4.7 Ga solar system, and recent space missions such as Hayabusa, Hayabusa2, and OSIRIS-REx have focused on carbonaceous asteroids, advancing our understanding of these ancient materials. It is also likely that in the next few years, there will be a significant increase in the regular collection of regolith samples and the return of more carbonaceous chondrite samples. Among these, the Vigarano meteorite, a CV3 carbonaceous chondrite that fell in 1910, is notable for its large chondrules, refractory inclusions (CAIs), and a matrix comprising 40% of its volume. Here, C indicates the carbon class, V the Vigarano group, and 3 petrographic types, respectively [6].

Carbonaceous chondrites contain Ca-Al (calcium-aluminum)-rich inclusions (CAI), and Vigarano-type carbonaceous meteorites are particularly important because they contain CAIs composed of high-temperature-resistant oxides and silicates. These rare and

DOI: https://doi.org/10.21205/deufmd.2026288312

Geliş Tarihi / Received: 10.02.2025
Kabul Tarihi / Accepted: 03.10.2025

valuable extraterrestrial materials are the first surviving solids to condense into the solar nebula, with a timescale of slightly over 4.5 Ga. NWA 5508 is rich in both CAIs and chondrules, making it invaluable for investigating the early solar nebula's environmental conditions [7].

CAIs shed light on events that occurred during the formation of the solar system and provide information about the time and environmental conditions in which these events occurred. CAIs, typically less than 1 mm but sometimes reaching up to 2-3 cm in CV3 chondrites [8-12], were first identified in the Vigarano meteorite in 1968 and later extensively studied in the Allende meteorite. For example, the Allende meteorite, a CV3 chondrite, contains between 5 and 10% CAIs by volume [13, 14].

In summary these inclusions, formed in high-temperature regions of the solar nebula, consist of complex minerals like melilite, spinel, and anorthite [15]. Their presence across all CV3 chondrites provides critical data on the environmental conditions and timelines of early solar system processes, emphasizing the importance of these extraterrestrial materials in planetary science.

2. Materials and Methods

Vigarano-type carbonaceous chondrite NWA 5508 (CV3) was found in Northwest Africa in 2008 [16]. The total mass of the NWA 5508 meteorite fragment used in petrography and scanning electron microscopy (SEM)-energy dispersive X-ray spectroscopy (EDS) analyses is approximately 19.34 g. This sample has a dark matrix, and it contains abundant CAIs and visible macroscopic chondrules. The polished section of NWA 5508 chondrite used in the analysis is given in Figure 1.

Figure 1. Analysis surface (left) and a back surface (right) of NWA 5508 polished section.

2.1. Sample Preparation

For the petrographic study performed with an optical microscope, a thin section of NWA 5508 meteorite was prepared by Dokuz Eylül University Geological Engineering Department in İzmir, Türkiye. First, the polished section of the meteorite was cut into slices and glued onto an Araldite slide. Then, to adjust the thickness of the cut meteorite sample to approximately 30 µm, its surface was abraded in several stages from coarse-grained abrasive to fine-grained abrasive. After the abrasion process, the surface of the meteorite sample was polished with a solution containing diamond particles, 10, 6, and 1 µm, respectively. As a result, a 4.8x2.8 cm thin section was obtained as depicted in Figure 2.

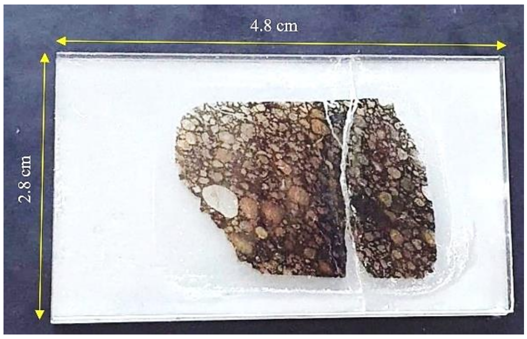

Figure 2. A thin section of NWA 5508.

Before SEM-EDS analysis and imaging, the air inside the thin section was vacuumed. After the vacuuming process, the analysis surface of the thin section was coated with Au for approximately 60 s. Then the thin section was glued onto double-sided carbon tape. After the bonding process on the carbon tape, it was placed in the SEM device compartment and vacuumed for 3 mins. before imagining. SEM images were obtained with the BSE (Backscattered Electron) detector to distinguish different phase structures. The EDS detector (EDAX) was used for elemental mapping together with the analysis of elemental spectra on the obtained BSE images. SEM-EDS analyses were performed using the Thermo Scientific Apreo S SEM device located at the Ege University Central Research Test and Analysis Laboratory Application and Research Center.

When the meteorite thin section is examined, the orientation and elongation of the CAIs are clearly visible. The NWA 5508 meteorite contains abundant chondrules and CAIs. However, CAI structures were selected for analysis because CAIs are the oldest solids in the solar system, and most of the fine-grained matrix material in chondrules and primitive chondrites formed 1-4 Myr after the CAIs. Therefore, seven elongated inclusion zones from the thin section were selected for petrography and SEM-EDS analyses [17]. Seven CAI regions (yellow marked) located in the thin section of the NWA 5508 carbonaceous chondrite were numbered and marked on the thin section prior to analysis (Figure 3). Each marked region was named CAI 1, CAI 2, CAI 3, CAI 4, CAI 5, CAI 6, and CAI 7.

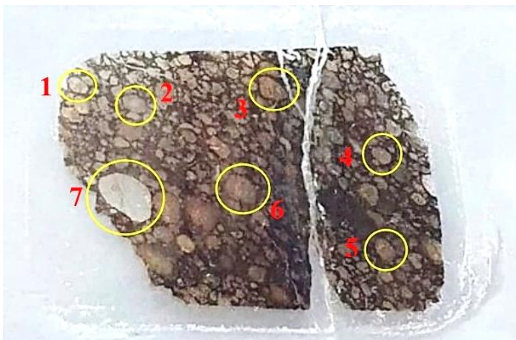

Figure 3. Locations of the studied CAIs in thin section.

2.2. Optical Microscopy (Petrography)

Petrographic analysis of the six CAI regions was performed with a bottom-illuminated polarizing microscope Leica DM750 P at Dokuz Eylül University Geological Engineering Department. Microscopic images of CAI structures in NWA 5508 were obtained as crossed light (cross-polarized light, XPL) and parallel light (plane-polarized light, PPL) using 1.5, 2.5, 4, and 63x objectives. Optical images obtained as XPL and PPL are given in Figures 4-11, respectively. The optical image of CAI 1 could not be obtained due to air bubbles formed during the repair of the thin section. The scales in the optical images are, respectively: 200 µm for Figures 4-7, 500 µm for Figure 8, 1 mm for Figure 9, and 50 µm for Figures 10-11. Olivine in the meteorite is identified by its high birefringence and distinctive cracks (Figures 4-8). Clinoenstatite in the meteorite is generally found around olivine and CAIs (Figures 4-5). It is identified by intersecting cracks at approximately 90° and the oblique extinction characteristic of clinopyroxene. The anorthite in the meteorite is identified by prominent polysynthetic twinnings within the central large structure and a characteristic oblique extinction angle of approximately 25-30° (Figure 9). Polysynthetic twinning indicates minerals belonging to the plagioclase group. In high-calcium plagioclases like anorthite, these twinnings appear as thinner, denser bands (Figure 9). Plagioclase in the meteorite has lower birefringence and relief than olivine, clinoenstatite, and apatite. It is identified by distinctive polysynthetic twinning (Figure 10). Apatite inclusions observed with plagioclase in the meteorite are identified by their high relief and prismatic-shape (Figure 11).

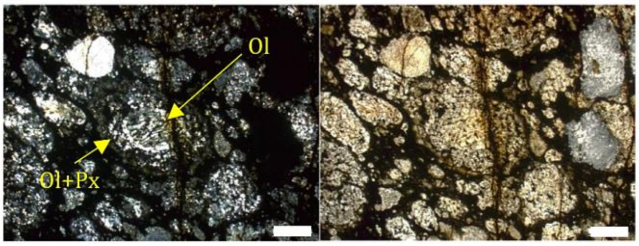

Figure 4. Barred olivine surrounded by a porphyritic olivine and pyroxene (clinoenstatite) mineral assemblage in CAI 2.

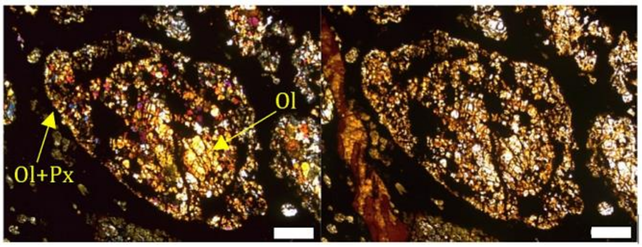

Figure 5. Another barred olivine surrounded by a mineral assemblage composed of porphyritic olivine and pyroxene (clinoenstatite) in CAI 3.

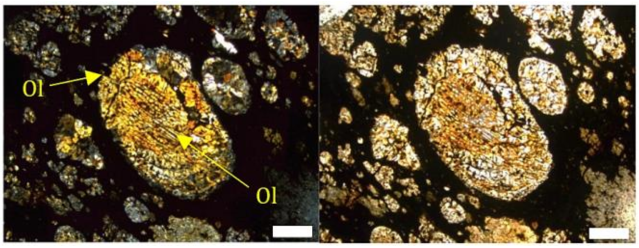

Figure 6. Barred olivine with glassy phases in between in CAI 4.

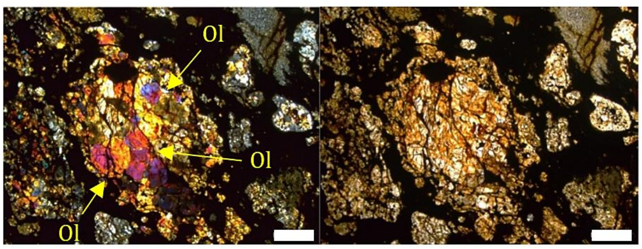

Figure 7. Coarse-grained dunite composed of porphyritic olivine in CAI 5.

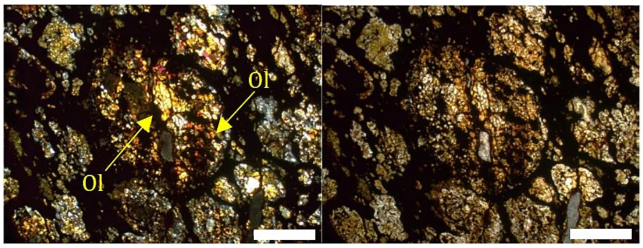

Figure 8. Porphyritic olivine of different shapes and sizes in CAI 6.

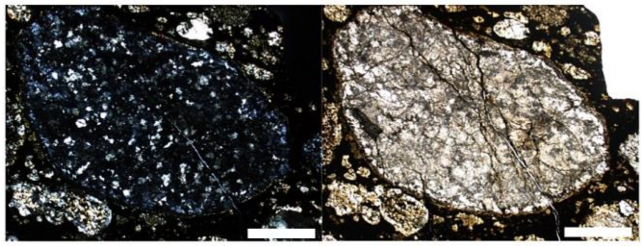

Figure 9. CAI 7 showing granular and microcrystalline texture (Anorthite).

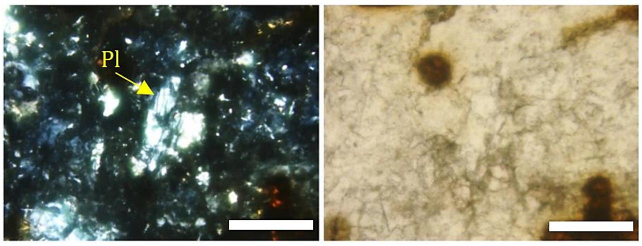

Figure 10. Plagioclase showing polysynthetic twinning in CAI 7.

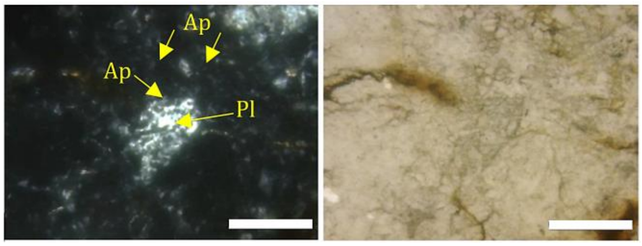

Figure 11. Another plagioclase shows prismatic-shaped apatite inclusions in CAI 7.

The preservation of barred olivine (BO) structures in optical microscopy analyses (especially CAI 2, 3, and 4) suggests an intact cooling texture (Figures 4-6). Well-preserved polysynthetic twinning observed in plagioclases (e.g., CAI 7) is consistent with low-grade thermal effects (Figure 10). However, in some structures (e.g., CAI 5), amorphous glass phases surrounded by olivine may indicate partial melting and recrystallization processes (Figure 7). To sum up, optical data show that low-grade heat exposure partially altered the texture in some areas of CAIs, but most of them retained their original structure.

2.3. Scanning Electron Microscopy - Energy Dispersive X-ray Spectroscopy

SEM-EDS analysis of the seven CAI regions was performed with a Thermo Scientific Apreo S SEM device located at the Ege University Central Research Test and Analysis Laboratory Application and Research Center. A Thermo Scientific Apreo S SEM equipped with an EDAX detector was used for mapping. Brightness and contrast were set to 46.50% and 54.32%, respectively for the BSE imaging. Images of these regions were obtained at 20 kV energy, 12.0 point size. Image resolution was set to 3072x2048, dwell time was set to 5 µs and working distance was set to 8.8 mm. Horizontal field width (HFW) was adjusted to 1.66 mm. 250 x magnification was set for the except region 5. HFW was set to 1.18 mm, and magnification was set to 350x for CAI 5 region. EDS mapping parameters were manually chosen to get optimal data collection. The resolution was set to 512x400, the frame was set to 64, and the dwell time was set to 150 µs. Based on these experimental conditions analyses for each CAI region took ~40 minutes. BSE images, EDS maps, and spectra are presented in Figures 12-18, and weight (wt.%) element tables are given in Tables 1-7, respectively.

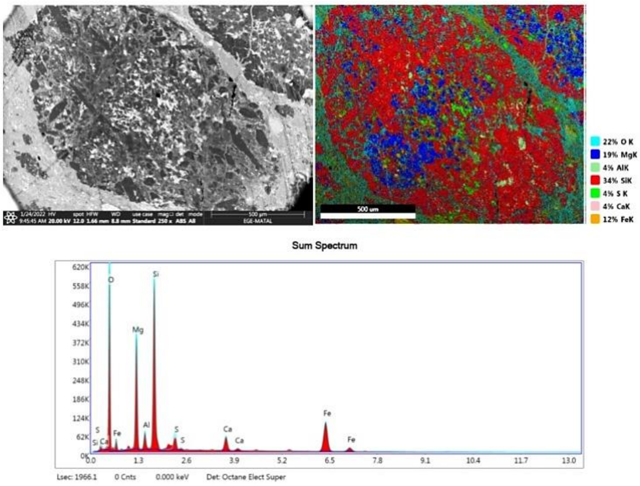

Figure 12. BSE image (top left), EDS map (top right) and spectrum (bottom) of CAI 1.

Table 1. Elemental percentage (%) distribution for CAI 1.

Element	Weight %	Atomic %
O K	38.33	54.93
MgK	16.21	15.29
AlK	2.45	2.08
SiK	21.29	17.38
S K	2.84	2.03
CaK	3.30	1.89
FeK	15.58	6.40

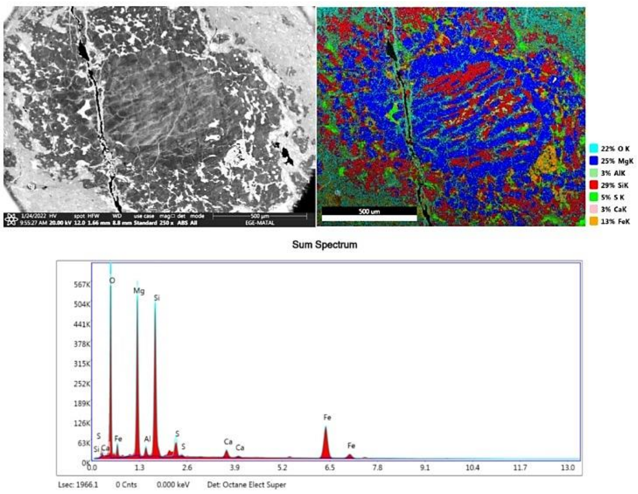

Figure 13. BSE image (top left), EDS map (top right) and spectrum (bottom) of CAI 2.

Table 2. Elemental percentage (%) distribution for CAI 2.

Element	Weight %	Atomic %
O K	36.18	52.18
MgK	21.88	20.76
AlK	1.32	1.13
SiK	19.31	15.86
S K	3.21	2.31
CaK	1.70	0.98
FeK	16.40	6.77

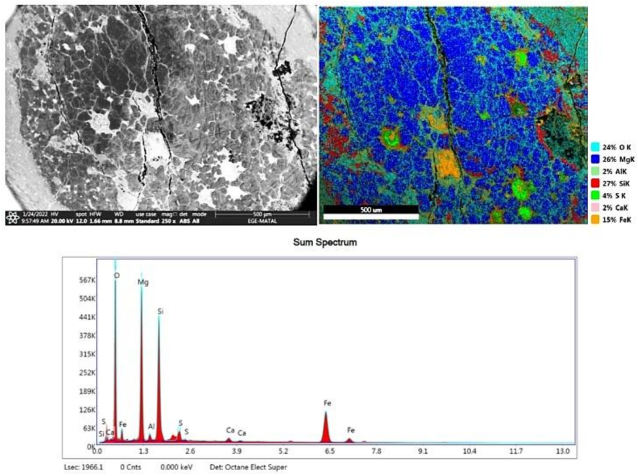

Figure 14. BSE image (top left), EDS map (top right) and spectrum (bottom) of CAI 3.

Table 3. Elemental percentage (%) distribution for CAI 3.

Element	Weight %	Atomic %
O K	35.78	51.79
MgK	23.70	22.58
AlK	1.08	0.93
SiK	17.93	14.78
S K	2.76	2.00
CaK	0.94	0.54
FeK	17.81	7.38

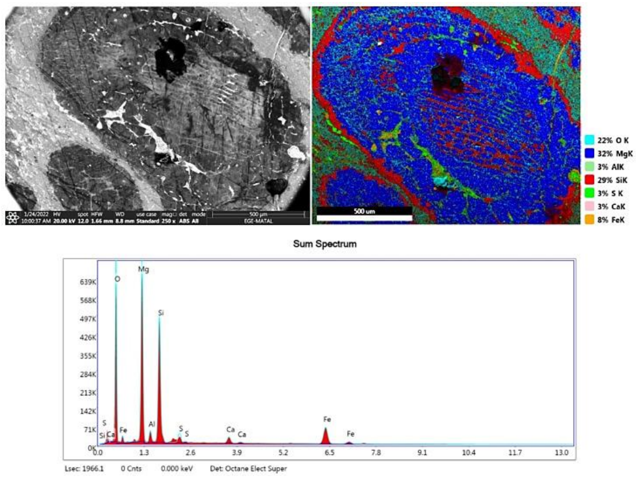

Figure 15. BSE image (top left), EDS map (top right) and spectrum (bottom) of CAI 4.

Table 4. Elemental percentage (%) distribution for CAI 4.

Element	Weight %	Atomic %
O K	37.57	52.12
MgK	26.29	24.00
AlK	1.98	1.63
SiK	19.91	15.74
S K	1.97	1.36
CaK	1.75	0.97
FeK	10.54	4.19

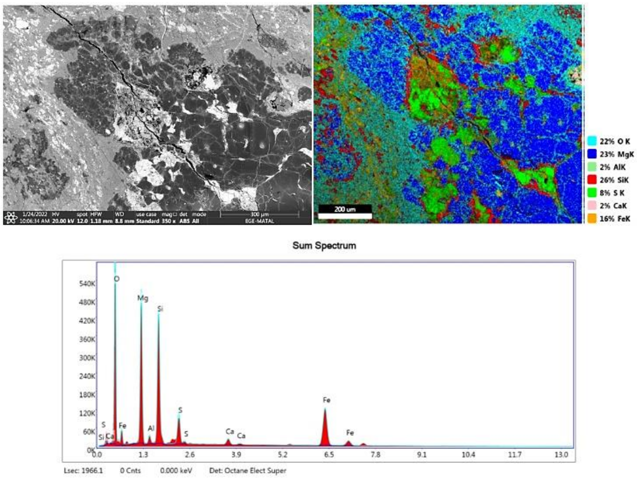

Figure 16. BSE image (top left), EDS map (top right) and spectrum (bottom) of CAI 5.

Table 5. Elemental percentage (%) distribution for CAI 5.

Element	Weight %	Atomic %
O K	34.90	51.59
MgK	20.75	20.18
AlK	1.17	1.03
SiK	16.94	14.26
S K	5.05	3.73
CaK	1.40	0.82
FeK	19.79	8.38

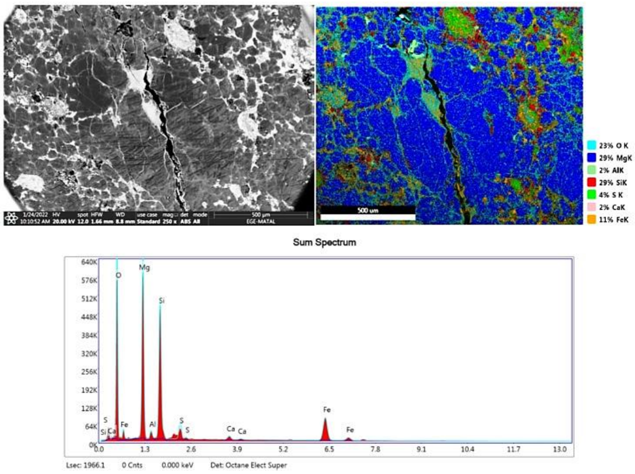

Figure 17. BSE image (top left), EDS map (top right) and spectrum (bottom) of CAI 6.

Table 6. Elemental percentage (%) distribution for CAI 6.

Element	Weight %	Atomic %
O K	36.86	51.99
MgK	25.02	23.23
AlK	1.24	1.04
SiK	19.56	15.72
S K	2.90	2.04
CaK	0.98	0.55
FeK	13.44	5.43

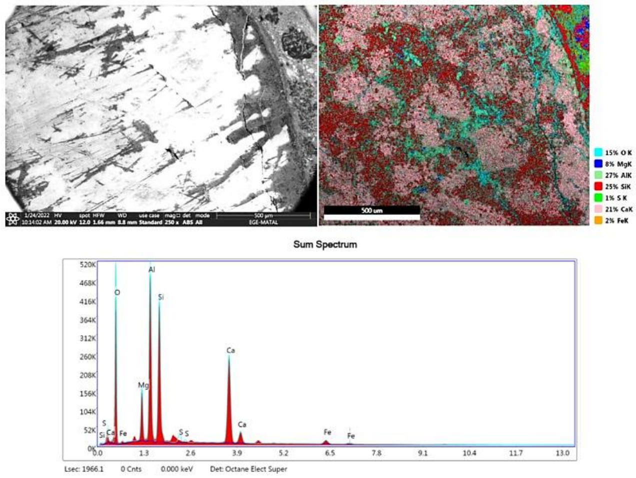

Figure 18. BSE image (top left), EDS map (top right) and spectrum (bottom) of CAI 7.

Table 7. Elemental percentage (%) distribution for CAI 7.

Element	Weight %	Atomic %
O K	42.43	58.45
MgK	5.53	5.01
AlK	16.83	13.75
SiK	15.04	11.80
S K	1.14	0.79
CaK	17.35	9.54
FeK	1.67	0.66

3. Results and Dicussion

The polished section of the NWA 5508 was physically examined and compared with other CV3 chondrites in the same group such as Allende, Bali, Efremovka, Kaba, Vigarano and Leoville. Based on the previous data, the first study on the determination of subgroups of CV3 chondrites by [18] stated that these meteorite types have a very heterogeneous structure and defined them as a complex meteorite class. At the same time, these carbonaceous chondrite types also differ in the matrix and chondrule ratios they contain [18, 19]. NWA 5508 has a fine-grained and almost opaque matrix, and it contains abundant chondrules of different sizes and CAIs. It also has a multi-type of matrix and very heterogeneous structure like other CV3 chondrites.

The sizes of the seven CAI structures found in NWA 5508 were calculated with the ImageJ program [20, 21]. The sizes of CAI 1, CAI 2, CAI 3, CAI 4, CAI 5, CAI 6, and CAI 7 structures were found to be 0.143 cm (1.43 mm), 0.199 cm (1.99 mm), 0.235 cm (2.35 mm), 0.150 cm (1.50 mm), 0.164 cm (1.64 mm), 0.243 cm (2.43 mm) and 0.458 cm (4.58 mm), respectively. The sizes reported of CAI structures found in other CV3 group meteorites were compared with the CAIs in NWA 5508 in Table 8.

Table 8. Benchmark of CAI sizes compared to NWA 5508.

Name	Size*	Reference
NWA 10758	*2.4×1.4 cm*	[8]
Allende	*~2 cm*	[9, 10]
Efremovka	~15 mm (*~1.5 cm*)	[11]
Allende	*2.5×1.5* and *1 cm*	
NWA 3118	*2, 1.7, 1.1, and ~1.5 cm*	[12]
Efremovka	**0.5** and *1 cm*	[22]
Kaba	0.20 mm	[23]
Bali	0.17 mm	
Allende	0.22 mm	
NWA 779	0.29 mm	
NWA 2900	0.36 mm	
Vigarano	10 mm (*1 cm*)	[24]
Vigarano	**4.7**, **4×5**, 2.2×2.8, 1.8×**4.8**, and ~6.2×**3.9** mm	[25]
Vigarano	**0.4×0.5** cm	[26]
Leoville	**>3**, 1.2, and 0.7 mm	[27]
RBT 04143	1.5×0.8, 0.7×0.4, 0.3×0.3, and 0.3×0.2 mm	[28]
Vigarano	*1.2 cm*, 2 and **5 mm**	[29]
Leoville	**~3 mm**	
Efremovka	**~3**×2 mm	
Allende	**~**7 mm	
Axtell	2×**3** mm	

***Italicized** values refer to CAIs of cm size (exception ≥1 cm) and values in **bold** are consistent with the size of the largest CAI (CAI 7) in NWA 5508 (≥3 to ≤5 mm).

According to the results obtained within the scope of the study on the sizes of CAIs of Vigarano by [25, 26], the CAI 7 structure with the largest diameter (~4.6 mm) in the NWA 5508 is compatible with the sizes of the three CAI structures. To sum up, the sizes of CAIs in NWA 5508 are compatible with the sizes of CAIs in other CV3 type chondrites and fit the general characteristics of the group of CV3 chondrites mentioned in Table 8. Size differences in CAI structures across meteorite samples are a common occurrence in literature, particularly when considering the formation conditions and thermal evolution processes of carbonaceous chondrites [8-12, 22-29]. Therefore, while inferences based solely on size similarity appear to be of limited value, the consistent pattern of CAI sizes highlighted in our study points to a specific origin (the likely parent body of the meteorite).

The dominant mineral in NWA 5508 is olivine. In addition, the presence of anorthite and plagioclase with apatite inclusions minerals was also observed in the meteorite. Similarly, when looking at the studies on CV3 chondrites in literature, it has been shown that the dominant mineral in such carbonaceous chondrites is olivine [30-34]. According to the literature, BO, which is a chondrule structure frequently seen in CV3 chondrites, was also observed in the NWA 5508 (Figure 6) [14].

According to the BSE images, EDS maps, EDS spectra, and weight (wt.%) results obtained from the seven CAI regions, the primary elements in the meteorite are Mg, Si, and Fe, while the secondary elements are Ca, Al, and S. CV3 chondrites have an olivine-rich mineralogy and a heterogeneous structure [32, 35-37]. In a study on the Allende chondrite, MgO, FeO, and SiO_2 were found to be 48.31, 7.84, and 43.44% by weight, respectively (wt.% of Mg, Fe, and Si elements were 29.13, 6.10, and 20.30%, respectively), and it was reported that forsterite, which is the Mg-bearing olivine in the meteorite content, was the primary mineral [35]. The Mg, Fe, and Si elements contained in the six CAI structures (CAI 1, CAI 2, CAI 3, CAI 4, CAI 5, and CAI 6) in the NWA 5508 chondrite vary between 16.21 and 26.29%, 10.59 and 19.79%, and 16.94 and 21.29% by weight, respectively (Tables 1-6). Consequently, based on the wt.% of Mg, Fe, and Si, the dominant mineral in the NWA 5508 chondrite is forsterite.

In addition, in the study by [38] on the Allende chondrite, anorthite, CaO, Al_2O_3, and SiO_2 were found to be 19.68, 31.57, and 47.49% by weight, respectively (the wt.% of Ca, Al, and Si elements were 14.07%, 16.71%, and 22.20%, respectively), and according to these results, anorthite, which is a Ca- and Al-bearing mineral, was defined as the secondary mineral in the meteorite [38]. Additionally, in the work by [39] on Allende and Bali chondrites, the Ca, Al, and Si elements have values varying between 1.44-3.75, 1.01-3.77, and 13.73-16.13% by weight for Allende, respectively, and the Ca, Al, and Si elements have values varying between 1.53-3.82, 0.93-5.97, and 12.41-13.05% by weight for Bali, respectively [39]. According to [14], CAI structures composed of high-temperature-resistant oxides and silicates have a complex structure mineralogically. The results of SEM-EDS analysis of the largest CAI structure (CAI 7) in NWA 5508 showed that this inclusion consists of anorthite (Calcium-Aluminum silicate). Other CAI structures are predominantly composed of Mg-bearing olivine (Forsterite).

Detailed SEM-EDS results of the elemental distribution of seven CAI structures obtained as a result of the analyses are as follows:

i. CAI 1 region has relatively higher Si and Mg than the matrix. The inner part of the inclusion contains locally higher Mg. The bright areas in the inclusion are rich in S. Fe is generally found in small dots and scattered throughout the inclusion with S (Figure 12).
ii. CAI 2 region has relatively higher Mg than the matrix. Si is present in the center of the inclusion with Al inside the Mg. It is also present in clusters at the periphery. Fe is present in the bright areas of the inclusion as small dots and generally in clusters with S. In addition, S is found scattered around the inclusion (Figure 13).
iii. CAI 3 region is rich in Mg. The bright areas in the inclusion are rich in S. S is scattered in the inclusion as islands with Fe. Fe is present in small dots and clusters inside the S and in some regions surrounding the S (Figure 14).
iv. CAI 4 region is rich in Mg. Si is present in the interior of the inclusion and in honeycombs surrounding the edges of Mg. In addition, the inclusion has a Si wall due to the contribution of S in dispersed form. The bright areas in the

inclusion are rich in S. Fe is present in small dots and clusters with S (Figure 15).

v. CAI 5 region is rich in Mg. The bright areas in the inclusion are rich in S. Fe is present in small dots and clusters inside S. Si is present in small dots generally surrounding Fe-S (Figure 16).

vi. CAI 6 region is rich in Mg. Fe and Si are generally found in dispersed form associated with S. In some regions, Fe is present in small dots and clusters inside S (Figure 17).

vii. CAI 7 region is rich in Ca and Al. Mg is present in small dots and clusters with Al in the inclusion, which is poor in Mg. Si is present in the interior of the inclusion as small dots and clusters and is present at the visible margin of the inclusion. The inclusion is poor in Fe-S compared to the other six inclusions (Figure 18).

In general, in these seven CAI structures, Fe and S are complementary to each other. There are Fe-S regions in clusters in most inclusions. CAI 7 region shows a Ca-Al-rich structure, unlike other inclusions. Most of the inclusions, except CAI 7 region, have a Mg-rich structure. According to SEM-EDS results, the inclusions in NWA 5508 have different and complex structures. According to the elemental percentage (%) distribution of Mg, Fe and Si in Tables 1-6, it was observed that the dominant mineral in CAI structures was olivine (forsterite). Additionally, microscopy and SEM-EDS images of the CAI 7 region, which is the largest CAI structure in the meteorite, revealed the presence of Ca-bearing plagioclase mineral (anorthite) and Mg-bearing olivine mineral (forsterite).

4. Conclusions

CV3 chondrites show various degrees of aqueous alteration and/or thermal metamorphism. Thermal metamorphism can be understood by distinguishing between various petrographic subtypes of chondritic meteorites. During thermal metamorphism, many changes occur in the textures of chondrites subgroups of CV3 chondrites are affected by these changes to different degrees. In contrast, there is little evidence of what kind of thermal metamorphism other carbonaceous chondrites have experienced, and therefore, more studies on carbonaceous meteorites are needed to have more information about the thermal history of carbonaceous chondrites [40]. In this study, CAI structures in the meteorite were examined petrographically by optical microscopy, and the mineralogy of these structures was revealed by SEM-EDS technique.

Mg-rich CAIs (CAIs 1-6) indicate the influence of short-term, low-grade thermal metamorphism. The Fe-S clusters, particularly prominent in some CAIs (CAIs 5 and 6), may have been displaced or partially recrystallized during cooling. CAI 7 is the region least affected by thermal metamorphism. This structure likely formed at high temperatures in the original nebular environment and was subsequently preserved at lower temperatures. Optical data indicate that the low-grade thermal effect has partially altered the textures in some regions of the CAIs, but most retain their original structure. Studies of CV3 meteorites such as Allende, Bali, and Efremovka indicate that CV3s can span a wide range of thermal metamorphic scales [7, 15, 19]. In this sense, NWA 5508 may have exhibited less thermal alteration than Allende but more than Bali. The Fe-S clusters and heterogeneous elemental distribution suggest that some CAIs were subjected to short-term post-nebular heat flows.

Consequently, the CAI structures in NWA 5508 show signs of very low-grade thermal metamorphism. The Mg/Fe/Si distributions indicate that most CAIs retain their forsteritic structure. High Ca-Al structures, such as CAI 7, stand out as refractory inclusions less affected by heat. Thermal metamorphism did not cause overall structural deterioration in the meteorite but rather caused local chemical redistributions.

In addition to all this, based on the findings of petrographic and SEM-EDS investigations of the NWA 5508 carbonaceous chondrite, it has been determined that the meteorite exhibits a heterogeneous structure characteristic of CV3 chondrites. The mineralogical composition predominantly consists of olivine, with notable inclusions of anorthite and plagioclase minerals containing apatite. Elemental analysis of the seven CAI regions revealed varying concentrations of Mg, Fe, and Si, identifying forsterite as the dominant mineral. Additionally, the largest CAI structure (CAI 7) displayed a unique Ca-Al-rich composition indicative of anorthite. These results align with known characteristics of CV3 chondrites, providing valuable insights into the early solar nebula's conditions and processes. It is clear that further studies are needed to determine the possible source body of both the NWA 5508 carbonaceous meteorite and other carbonaceous meteorites. In particular, understanding the underlying mechanism of thermal and/or aqueous alteration processes in these meteorites and the possible source body will provide important information on many subjects, such as the history of the solar nebula, protoplanetary disks, and the formation and evolution of planets.

Ethics committee approval and conflict of interest statement

This article does not require ethics committee approval. This article has no conflicts of interest with any individual or institution.

Acknowledgments

Ceren Kamil and Ozan Unsalan acknowledge Prof. Dr. Osman Candan of Dokuz Eylül University, Izmir, Türkiye for preparing the thin section of the NWA5508 chondrite. This research was funded by the Ege University Scientific Research Projects Coordination Unit under Project Number FDK-2021-22924 within the framework of Kamil's Ph.D. thesis.

Author Contribution Statement

Ceren Kamil: Execution of optical microscopy (petrography) analyses; SEM-EDS experimental work; data collection and processing; quantitative elemental analysis; preparation of figures, tables, and images; literature review; and drafting of the manuscript.

Ozan Unsalan: Study conceptualization and supervision; experimental design; interpretation of petrographic and SEM-EDS results; critical review and validation of analytical data; scientific editing of the manuscript; and final approval of the article.

Osman Candan: Preparation of the thin section at Dokuz Eylül University; guidance in petrographic observations; and technical support during optical microscopy analyses.

Ethics committee approval and conflict of interest statement

This article does not require ethics committee approval. This article has no conflicts of interest with any individual or institution.

Generative AI (Artificial Intelligence) Usage

Authors declare that none of generative AI tools were used for the paper preparation process.

References

[1] Varela ME, Métrich N. Carbon in olivines of chondritic meteorites. Geochim Cosmochim Acta 2020;64:3433-3438. doi:10.1016/S0016-7037(00)00432-4.

[2] Buseck Center for Meteorite Studies. Available from: https://meteorites.asu.edu/chondrites [Accessed 20 July 2025].

[3] Fraknoi A, Morrison D, Wolff S. Voyages Through the Universe. Harcourt; 2000.

[4] Koga T, Naraoka HA. A new family of extraterrestrial amino acids in the Murchison meteorite. Sci Rep 2017;7:636. doi:10.1038/s41598-017-00693-9.

[5] Pizzarello S, Cooper G, Flynn G. The nature and distribution of the organic material in carbonaceous chondrites and interplanetary dust particles. In: Lauretta DS, McSween HY Jr, editors. Tucson: University of Arizona Press; 2006, 625-651. doi:10.2307/j.ctv1v7zdmm.36.

[6] Meteoritical Bulletin Database. Available from: https://www.lpi.usra.edu/meteor/metbullclass.php?sea=CV3 [Accessed 20 July 2025].

[7] Bonal L, Quirico E, Bourot-Denise M. Petrologic type of CV3 chondrites as revealed by Raman spectroscopy of organic matter. In: 35th Lunar and Planetary Science Conference, League City, Texas; 2004. doi:10.1016/j.gca.2005.12.004.

[8] Zolensky M, Han J, Le L, Unsalan O, Altunayar-Unsalan C, Buchanan P. A rather thick, multilayered, accretionary rim on a rather large CAI in the NWA 10758 CV3 chondrite. In: 86th Annual Meeting of the Meteoritical Society (METSOC), Los Angeles, California; 2023.

[9] Aléon J. Oxygen isotopes in the early protoplanetary disk inferred from pyroxene in a classical type B CAI. Earth Planet Sci Lett 2016;440:62-70. doi:10.1016/j.epsl.2016.02.007.

[10] Aléon J. Closed system oxygen isotope redistribution in igneous CAIs upon spinel dissolution. Earth Planet Sci Lett 2018;482:324-333. doi:10.1016/j.epsl.2017.11.027.

[11] Bullock ES, MacPherson GJ, Nagashima K, Krot AN, Petaev MI, Jacobsen SB, Ulyanov AA. Forsterite-bearing type B refractory inclusions from CV3 chondrites: From aggregates to volatilized melt droplets. Meteorit Planet Sci 2012;47:2128-2147. doi:10.1111/j.1945-5100.2012.01396.x.

[12] Lorenz C, Ivanova M, Krot A, Shuvalov V. Formation of disk- and bowl-shaped igneous Ca,Al-rich inclusions: Constraints from their morphology, textures, mineralogy and modelling. Geochemistry 2019;79. doi:10.1016/j.chemer.2019.07.005.

[13] Christophe Michel-Lévy M. Un chondre exceptionnel dans la météorite de Vigarano (in French). Bull Mineral 1968;91:212-214.

[14] Norton RO, Chitwood LA. Field guide to meteors and meteorites. Springer; 2008. doi:10.1007/978-1-84800-157-2.

[15] MacPherson GJ, Simon SB, Davis AM, Grossman L, Krot AN. Calcium-Aluminum-rich inclusions: Major unanswered questions. In: ASP Conference Series, Kauai, Hawaii; 2005, 341.

[16] Meteoritical Bulletin Database. Available from: https://www.lpi.usra.edu/meteor/metbull.php?code=49208 [Accessed 2 September 2025].

[17] Krot AN, Amelin Y, Bland P, Ciesla FJ, Connelly J, Davis AM, Huss GR, Hutcheon ID, Makide K, Nagashima K, Nyquist LE, Russell SS, Scott ERD, Thrane K, Yurimoto H, Yin QZ. Origin and chronology of chondritic components: A review. Geochim Cosmochim Acta 2009;73:4963-4997. doi:10.1016/j.gca.2008.09.039.

[18] McSween HY Jr. Petrographic variations among carbonaceous chondrites of the Vigarano type. Geochim Cosmochim Acta 1977;41:1777-1790. doi:10.1016/0016-7037(77)90210-1.

[19] Krot AN, Scott ERD, Zolensky ME. Mineralogical and chemical modification of components in CV3 chondrites: Nebular or asteroidal processing?. Meteoritics 1995;30:748-775. doi:10.1111/j.1945-5100.1995.tb01173.x.

[20] Abramoff MD, Magalhaes PJ, Ram SJ. Image processing with ImageJ. Biophoton Int 2004;11:36-42.

[21] Schneider CA, Rasband WS, Eliceiri KW. NIH image to ImageJ: 25 years of image analysis. Nat Methods 2012;9:671-675. doi:10.1038/nmeth.2089.

[22] Amelin Y, Krot AN, Hutcheon ID, Ulyanov AA. Lead isotopic ages of chondrules and calcium-aluminum-rich inclusions. Science 2002;297:1678-1683. doi:10.1126/science.1073950.

[23] Chaumard N, Devouard B, Bouvier A, Wadhwa M. Metamorphosed calcium-aluminum-rich inclusions in CK carbonaceous chondrites. Meteorit Planet Sci 2014;49:419-452. doi:10.1111/maps.12260.

[24] Wark DA, Boynton WV. The formation of rims on calcium-aluminum-rich inclusions: Step I—Flash heating. Meteorit Planet Sci 2001;36:1135-1166. doi:10.1111/j.1945-5100.2001.tb01949.x.

[25] MacPherson GJ, Kita NT, Ushikubo T, Bullock ES, Davis AM. Well-resolved variations in the formation ages for Ca-Al-rich inclusions in the early Solar System. Earth Planet Sci Lett 2012;331-332:43-54. doi:10.1016/j.epsl.2012.03.010.

[26] Bullock ES, Knight KB, Richter FM, Kita NM, Ushikubo T, MacPherson GJ, Davis AM, Mendybaev RA. Mg and Si isotopic fractionation patterns in types B1 and B2 CAIs: Implications for formation under different nebular conditions. Meteorit Planet Sci 2013;48:1440-1458. doi:10.1111/maps.12158.

[27] Patzer A, Hezel DC, Bendel V, Pack A. Chondritic ingredients: II. Reconstructing early solar system history via refractory lithophile trace elements in individual objects of the Leoville CV3 chondrite. Meteorit Planet Sci 2018;53:1391-1412. doi:10.1111/maps.13084.

[28] Yoshizaki T, Nakashima D, Nakamura T, Park C, Sakamoto N, Ishida H, Itoh S. Nebular history of an ultrarefractory phase bearing CAI from a reduced type CV chondrite. Geochim Cosmochim Acta 2019;252:39-60. doi:10.1016/j.gca.2019.02.034.

[29] MacPherson GJ, Huss GR, Davis AM. Extinct 10Be in type A calcium-aluminum-rich inclusions from CV chondrites. Geochim Cosmochim Acta 2003;67:3165-3179. doi:10.1016/S0016-7037(02)01298-X.

[30] Kornacki AS, Wood JA. The mineral chemistry and origin of inclusion matrix and meteorite matrix in the Allende CV3 chondrite. Geochim Cosmochim Acta 1984;48:1663-1667. doi:10.1016/0016-7037(84)90335-1.

[31] Morlok A, Köhler M, Grady MM. Mid-infrared spectroscopy of refractory inclusions (CAIs) in CV and CO chondrites. Meteorit Planet Sci 2008;43:1147-1160. doi:10.1111/j.1945-5100.2008.tb01119.x.

[32] Szurgot M, Polański K. Microstructure of NWA 4435 meteorite. Sci Bull Tech Univ Lodz Phys 2008;29:75-83.

[33] Tomeoka K, Ohnishi I. Olivine-rich rims surrounding chondrules in the Mokoia CV3 carbonaceous chondrite: Further evidence for parent-body processes. Geochim Cosmochim Acta 2014;137:18-34. doi:10.1016/j.gca.2014.04.004.

[34] Futó P, Vanyó J, Simonia I, Sztakovics J, Nagy M, Gucsik A, Döncző B, Kertész Z, Novák R, Csámer A. The Mg/Fe ratio of silicate minerals in meteoritic materials and in the circumstellar environment: A case study for chondritic-like composition. Open Astron 2021;30:45-55. doi:10.1515/astro-2021-0006.

[35] Gucsik A, Endo T, Nakazato E, Nishido H, Ninagawa K, Kayama M, Bérczi Sz, Nagy Sz, Ábrahám P, Kimura Y, Gyollai I, Simonia I, Rózsa P, Posta J, Nagy M, Mihályi K, Apai D, Futó P. Cathodoluminescence characterization of the forsterite in Kaba meteorite: An astromineralogical application. In: 42nd Lunar and Planetary Science Conference, Houston, Texas; 2011.

[36] Dirri F, Ferrari M, Palomba E, Stefani S, Longobardo A, Rotundi A. Chondrules alteration study of NWA 2086 CV3 meteorite by using μ-IR and SEM/EDS combined analysis and implications for asteroid parent body. In: European Planetary Science Congress, Berlin, Germany; 2018.

[37] Kayastha R, Paul R, Stokke A. Comparative study of carbonaceous meteorites using micro-Raman spectroscopy and SEM/EDS. In: Proceedings of the National Conference on Undergraduate Research, Kennesaw, Georgia; 2019.

[38] Wesełucha-Birczyńska A, Żmudzka M. Micro-Raman spectroscopy characterization of selected meteorites. J Mol Struct 2008;887:253-261. doi:10.1016/j.molstruc.2008.01.029.

[39] Paul R. Comparative study of CV3 carbonaceous chondrites Allende and Bali using micro-Raman spectroscopy and SEM/EDS. Mankato, Minnesota: Minnesota State University; 2018.

[40] Huss GR, Rubin AE, Grossman JN. Thermal metamorphism in chondrites. In: Lauretta DS, McSween HY Jr, editors. Tucson, Arizona: University of Arizona Press; 2006, 567-586.